

# Online unsupervised Hebbian learning in deep photonic neuromorphic networks

**Authors:** Xi Li<sup>1</sup>, Disha Biswas<sup>2</sup>, Peng Zhou<sup>2</sup>, Wesley H. Brigner<sup>2</sup>, Anna Capuano<sup>3</sup>, Joseph S. Friedman<sup>1\*</sup>, Qing Gu<sup>1,4,\*</sup>

## Affiliations:

<sup>1</sup>Department of Electrical and Computer Engineering, North Carolina State University, Raleigh, NC 27695, USA

<sup>2</sup>Department of Electrical and Computer Engineering, The University of Texas at Dallas, Richardson, TX 75080, USA

<sup>3</sup>Department of Materials Science and Engineering, North Carolina State University, Raleigh, NC 27695, USA

<sup>4</sup>Department of Physics, North Carolina State University, Raleigh, NC 27695, USA

\*Corresponding authors. Email: \*qgu3@ncsu.edu (Q.G), joseph.friedman@utdallas.edu (J.S.F)

**Abstract:** While software implementations of neural networks have driven significant advances in computation, the von Neumann architecture imposes fundamental limitations on speed and energy efficiency. Neuromorphic networks, with structures inspired by the brain's architecture, offer a compelling solution with the potential to approach the extreme energy efficiency of neurobiological systems. Photonic neuromorphic networks (PNNs) are particularly attractive because they leverage the inherent advantages of light, namely high parallelism, low latency, and exceptional energy efficiency. Previous PNN demonstrations have largely focused on device-level functionalities or system-level implementations reliant on supervised learning and inefficient optical-electrical-optical (O-E-O) conversions. Here, we introduce a novel purely photonic deep PNN architecture that can revolutionize optical computation by enabling online, unsupervised learning. We propose a local feedback mechanism within the optical domain that implements a Hebbian learning rule on non-volatile phase-change material synapses. We experimentally demonstrate this approach on a non-trivial letter recognition task using a commercially available fiber-optic platform and achieve a 100% recognition rate, showcasing an all-optical solution for efficient, real-time information processing. Thus, this work unlocks the potential of photonic computing for complex artificial intelligence applications by enabling direct, high-throughput processing of optical information without intermediate O-E-O signal conversions.

## 1. Introduction

In the era of big data and artificial intelligence (AI), the demand for high-performance, energy-efficient computing solutions has surged. Neuromorphic computing, inspired by the structure and function of the human brain, offers a promising paradigm to address this demand<sup>1</sup>. With hardware that replicates the functionality of synapses and neurons in the brain and can be integrated into scalable networks, neuromorphic computing overcomes the data-transfer limitations of conventional von Neumann architectures. This approach enables highly parallel operation, energy-efficient and event-driven computation, inherent scalability, and stochasticity<sup>2-4</sup>.

While electronic neuromorphic networks have made significant strides<sup>5-12</sup>, photonic neuromorphic networks (PNNs) hold the transformative potential to revolutionize computing by leveraging the speed and energy efficiency of light-based computation<sup>13</sup>. Despite noteworthy

advancements in PNNs<sup>14-21</sup>, several previous limitations continue to hinder their advancement and adoption, particularly in optical-electrical-optical (O-E-O) conversions, reprogrammable storage of non-volatile synaptic weights, and the lack of online learning.

Most PNN inference circuits employ optical signals that flow through synapses and are converted to the electrical domain by neurons, before being converted back to the optical domain for propagation to the next layer of synapses<sup>19</sup>. These O-E-O conversions have significant energy and area costs, involving multi-stage signal processing that includes readout, amplification, and re-encoding onto optical signals between layers<sup>22</sup>. In addition to their inference costs, previous O-E-O conversions in learning circuits are extremely difficult to circumvent and require a purely photonic learning mechanism integrated into the deep PNN (DPNN) architecture. All of these O-E-O conversions undermine the speed and energy advantages achievable through DPNN computation<sup>13</sup>.

Adding to this challenge is the absence of robust, reprogrammable, non-volatile optical memory, as well as scalable, integrated hardware optical neurons, which further constrain the achievable complexity and functionality of current PNN architectures. Existing photonic synapse implementations – including micro-ring resonators<sup>23</sup>, Mach-Zehnder interferometers<sup>15</sup>, and beam splitters in a homodyne detection scheme<sup>24</sup> – share a significant drawback: inherent volatility that demands constant external biasing or power supply. Alternative approaches that do not require constant application of external energy fix synaptic weights during fabrication, and these weights cannot be modified later during learning.

In terms of network training, a key challenge lies in their limited online learning capabilities<sup>25</sup>. Existing PNNs predominantly rely on offline training on digital computers, followed by weight mapping<sup>26</sup>, pre-training of a digital twin<sup>27</sup>, or online training using peripheral electronic circuits<sup>28</sup>. Prior research has explored various strategies to address the limitations of backpropagation in supervised learning, including alternative gradient descent methods<sup>29,30</sup> and direct feedback alignment<sup>31</sup>. While these approaches offer some promise, they are difficult to implement solely in the optical domain. Moreover, the reliance of supervised learning on large, labeled datasets significantly restricts DPNN's applicability in many real-world scenarios. Pioneering efforts in implementing biological spike-timing-dependent plasticity (STDP)-based unsupervised online learning<sup>32</sup> show promise but do not yet extend to deep/multi-layer networks.

To overcome these challenges and unlock the true potential of PNNs, we propose a novel all-optical DPNN that maximizes computational efficiency and enhances learning dynamics through unsupervised online learning. Unlike supervised learning approaches that require large, labeled datasets, our unsupervised learning eliminates the requirement for labeled data<sup>33</sup> and avoids differential computations that demand on-chip electronics. Our architecture utilizes phase-change materials (PCMs) for both synaptic and neuronal functionalities, enabling highly efficient non-volatile operation with synaptic plasticity<sup>28,34-41</sup>. The proposed DPNN architecture offers three key advantages: I: Fully optical operation that maximizes energy efficiency and computational speed by eliminating O-E-O conversions that cause latency and high energy consumption; II: Unsupervised online learning capabilities that remove dependencies on labeled datasets and complex backpropagation algorithms; III: Implementation of a local Hebbian learning rule that significantly simplifies computational processes and reduces overhead. Our approach envisions a combination of best-in-class material and device platforms for both passive and active components, thereby overcoming the challenges faced by previous PNNs (Table 1). To validate our framework, we constructed a proof-of-concept network utilizing commercially available fiber-optic components. By performing a non-trivial letter recognition task, we demonstrated our network's proficiency in both supervised and unsupervised learning scenarios, achieving a 100% recognition rate. Our experimental results validate the proposed DPNN architecture, laying the groundwork for its future on-chip implementation and integration into large-scale photonic computing platforms.

We believe this work marks a decisive paradigm shift away from electronic neuromorphic chips and state-of-the-art PNNs for ultra-high-speed AI hardware.

Table 1 Summary of state-of-the-art PNNs.

PNN	DNN ( $\geq 3$ )	All-optical neuron	Reconfigurable synapse	On- chip	Online learning	Supervise d learning	Unsupervis ed learning
D <sup>2</sup> NN <sup>16</sup>	✓	✓				✓	
CNN(CMD) <sup>42</sup>	2 DMDs	PC	✓		Offline emulation	✓	
Single layer (PCM) <sup>17</sup>	1	✓	✓	✓	Single neuron	✓	✓
PDNN (PIN attenuator) <sup>43</sup>	✓	o-e-o	✓	✓	On-chip output as expected value	✓	
ONN (MZI) <sup>15</sup>	2 layers	PC	✓	✓		✓	
Tensor core (PCM) <sup>18</sup>	1 kernel	PC	✓	✓		✓	
Our experiment	✓	PC (emulation)	✓		✓	✓	✓
Our vision	✓	✓	✓	✓	✓	✓	✓

## 2. DPNN architecture

Our DPNN, depicted in Fig. 1a, is a multilayer neuromorphic network designed for both inference and unsupervised online learning. A key innovation is the implementation of optically controlled PCM synapses and PCM microring neurons (Fig. 1b(I)), featuring a local feedback mechanism that enables all-optical neuromorphic computation with unsupervised learning. This fundamentally distinguishes our approach from previous PNNs, which rely on global backpropagation and require complex electronic components for gradient computation. Our design of a local feedback circuit eliminates the dependence on external electronics during learning, thereby significantly reducing system complexity and enhancing scalability. In addition, this approach enables efficient weight updates directly in the optical domain, thereby avoiding the latency and energy costs associated with data transfer between the optical and electrical domains.

During inference, the network applies previously learnt synaptic weights for vector-matrix multiplication. Within each row of the crossbar, input optical signals are evenly distributed to the PCM optical synapses via directional couplers with precisely controlled coupling lengths (Fig. 1b(IV)). PCMs exhibit high contrast in optical properties, namely, refractive index and distinction coefficient, between their crystalline and amorphous phases and can be switched at nanosecond timescales with high reproducibility<sup>34</sup>. Furthermore, their states demonstrate high stability for years at normal operating temperatures, fulfilling a crucial requirement for practical non-volatile memory<sup>35,36</sup>. Thus, the utilization of PCM optical synapses can minimize energy consumption during both inference and idle states<sup>37-41,44</sup>. Additionally, waveguide crossings can be designed to minimize circuit footprint, crosstalk, and insertion loss across a broad optical bandwidth (Fig. 1b(III))<sup>45</sup>.

Along each column, the distributed signals from all rows are combined into an optical input/pump signal that drives the PCM microring neurons (Fig. 1c(II)). In the neuron's initial state, the PCM is crystalline, and the microring is designed to be critically coupled to the bus waveguide. In this condition, the internal losses perfectly match the coupling strength, trapping and dissipating the probe signal almost entirely within the ring, resulting in a 'low' or 'off' output. When the integrated pump signal intensity exceeds a threshold, the PCM cell atop the

microring undergoes a phase transition from the crystalline to the amorphous state. This transition triggers two simultaneous effects: 1. Shift in the resonant wavelength: the effective refractive index at the operating wavelength near 1550 nm decreases, shifting the microring resonance to shorter wavelengths. 2. Coupling modulation: the reduced absorption of the amorphous phase lowers the round-trip loss, driving the microring–bus waveguide system from critical coupling into the over-coupled regime. Together, these effects detune the microring from the probe wavelength, allowing the probe light to transmit through the bus waveguide rather than being absorbed. As a result, the output signal increases monotonically with the degree of amorphization, and therefore with the pump intensity.

This sudden increase in the transmission of the probe signal – from on-resonance to off-resonance with the micro-ring – constitutes the neuron’s “firing” event, producing an input-output response that closely resembles a rectified linear unit (ReLU) activation function<sup>17</sup>. The neuron output signal is then amplified by a semiconductor optical amplifier (SOA) and split to serve as input signals into the next layer (Fig. 1c(II)) and feedback signals for local learning. To reset the neuron between inferences, a staircase-shaped optical pulse is to be delivered via the adjacent vertical bus waveguide. This pulse, modulated to induce controlled recrystallization, returns the PCM to its initial fully crystalline state for the next iteration of inference.

Whereas the local feedback path is deactivated during inference by an electrically controlled PCM switch (ePCM in Fig. 1b(II)), the local feedback is activated during training, with the feedback signal evenly distributed to all matrix cells within the same column. When the input pulses are sufficiently long to temporally overlap with the feedback pulse at the optically controlled PCM (oPCM) synapse positioned atop the waveguide crossing in each matrix cell (Fig. 1c(I)), the PCM phase changes incrementally, enabling continuous synaptic weight adjustment and network adaptation. The synaptic weight update is realized through this local feedback structure, based on a simplified Hebbian learning rule<sup>46,47</sup>, embodying the neurobiological principle of “cells that fire together wire together”.

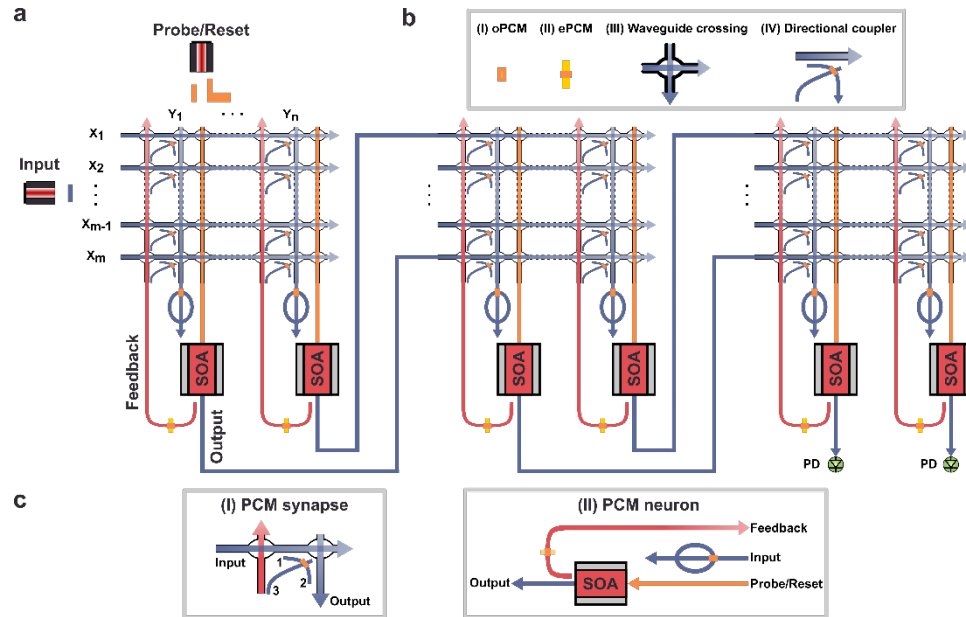


Fig. 1 System-level diagram of the DPNN. (a) Multilayer photonic crossbar architecture composed of non-volatile PCM cells. In each crossbar, an optical input vector is multiplied by a PCM synaptic weight matrix and summed along each column. Arrows indicate signal flow direction, with color gradients representing signal power distribution and integration. (b) Key components of the system: optically controlled PCM cells (oPCM) implement synapses and neurons, while electrically controlled PCM cells (ePCM) activate or deactivate the local feedback loops. Inverse-

designed waveguide crossings minimize row-column signal crosstalk, and directional couplers with varying coupling ratios ensure equal input power distribution to each PCM synapse (with its power adjusted to prevent PCM phase transitions during inference). (c) Major function blocks: (I) In each PCM synapse, input (blue) and feedback (red) signals from two directional couplers (1 and 3) overlap at the waveguide crossing when the local feedback is activated during training; (II) In the PCM neuron, the integrated post-synaptic signal is injected into an all-pass filter via a straight waveguide intersecting the microring resonator. When the integrated post-synaptic signal power exceeds a threshold, the PCM cell atop the ring resonator switches state, shifting its resonance and modulating the coupling condition. Thus, the bus waveguide on the bottom becomes detuned with the ring, generating an output pulse (blue) from the probe signal (orange). The SOA amplifies the neuron's output and sets both feedback and output signals to proper levels, enabling layer-to-layer cascading in deep photonic neural networks.

### 3. Hebbian learning with PCM synapses

Our DPNN architecture leverages the inherent plasticity of PCM optical waveguide synapses to enable unsupervised Hebbian learning. We choose germanium-antimony-tellurium (GST) compounds as the PCM candidate in our design due to their non-volatile yet reconfigurable nature, which allows dynamic and persistent synaptic weight adjustments. The phase transition dynamics of GST, governed by temperature-related thresholds, including the glass transition and melting temperatures, provide precise control over GST's optical properties<sup>48,49</sup>. This temperature-dependent phase dynamics, coupled with the material's crystal-growth-rate characteristics, provides a robust mechanism for implementing synaptic plasticity. A key attribute of GST, and PCMs in general, is their inherent hysteresis, which ensures that the phase transition is not solely determined by the instantaneous optical input but also by the present synaptic state.

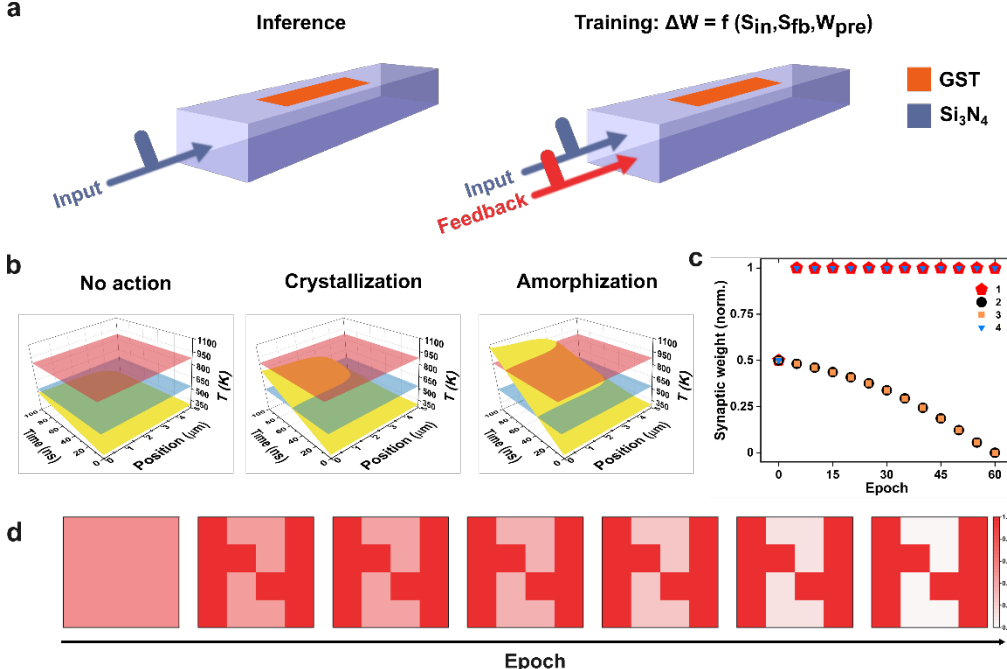


Fig. 2 PCM synapse operation and learning dynamics. (a) Schematic of the PCM synapse, illustrating that phase transitions in GST during training are induced by the temporal overlap of input and feedback signals, not by input alone. (b) Spatiotemporal temperature profile within the GST cell along the waveguide. The blue and red planes represent the glass transition and melting temperatures, respectively. When the yellow plane does not intersect either the red or blue plane, the synaptic weight is not updated; when the yellow plane intersects only the blue plane, crystallization occurs, and the synaptic weight is decremented; when the yellow plane intersects the red plane, amorphization occurs, and the synaptic weight is reset to a high state. (c) Synaptic weight evolution during learning for the four pixels in the first row of the letter 'N,' starting from a half-amorphous initial state. (d) Temporal evolution of the synaptic weights of the network, showing the encoding of the 'N' pattern.

Exploiting this unique attribute, we developed a synaptic weight updating scheme that closely mimics the biological STDP mechanism, enabling unsupervised Hebbian learning in the optical domain. In our photonic implementation, this translates into potentiation or depression of synaptic weights based on the temporal overlap of optical signals representing pre- and post-synaptic activities. During training, the coincident arrival of an input optical pulse and a local optical feedback pulse at the PCM synapse (Fig. 2a) induces a temperature rise of the GST material. The spatiotemporal temperature distribution within the PCM cell, modeled using a 1D heat equation (see Supplementary Information for details of the thermal model), is a function of the input pulse, feedback pulse, and the current synaptic weight (Fig. 2b). The relationship between this temperature profile and GST's characteristic transition temperatures dictate the direction and magnitude of the synaptic weight update. Specifically, sufficient heating above the crystallization temperature promotes a transition towards the crystalline state (weight decrement), while heating above the melting temperature, followed by rapid quenching, leads to the amorphous state (weight reset to a high value). If the thermal energy is insufficient to trigger a phase transition, the synaptic weight remains unchanged. A detailed description of this optically controlled synaptic weight updating mechanism is provided in Supplementary Information Fig. S1.

To elucidate the Hebbian learning capabilities of our PCM optical synapses, we analytically performed an unsupervised information encoding task using a pixelated single-letter image, as a precursor to proof-of-concept experiments that learn multiple patterns. We implemented the local feedback mechanism that routes a portion of the neuron's output signal back to the PCM synapses to overlap with the input signals. This creates a physical realization of the Hebbian principle of "neurons that fire together, wire together," where connections among inputs contributing to an output pulse are strengthened, while those that did not contribute are weakened.

During repeated presentations of the letter "N", the intensity of each pixel was mapped to the initial transmission of its corresponding PCM synapse. Driven by the local optical feedback, the synaptic weights evolved autonomously to encode the letter "N" without the need for an external supervisor. Fig. 2c and 2d illustrate this evolution, confirming that the unsupervised Hebbian process successfully captures the information encoding of the input pattern. By scaling the number of inputs, neurons, and layers, this architecture can be adapted to resolve increasingly complex tasks we demonstrated in section 4, showcasing the potential of DPNN for real-time, unsupervised learning within the photonic domain.

#### 4. Experimental Proof-of-Concept

We experimentally validated our design using a fiber-optics testbed, which, to the best of our knowledge, is the first demonstration of unsupervised online learning in a DPNN. While these initial experiments were conducted on a relatively small network with a limited number of neurons, they serve as a critical proof-of-concept, showing the feasibility of our approach and laying a strong foundation for future scaling to larger integrated photonic networks.

As illustrated in Fig. 4, our experimental setup comprises four key functional modules. I. Signal encoding: Input signals are generated using a telecom C-band continuous wave (CW) laser. Pixel information is encoded onto the optical carrier by amplitude modulation using variable optical attenuators (VOAs). II. Synaptic attenuation and weight updating: Synaptic weights are physically encoded using four VOAs arranged in a  $2 \times 2$  configuration, functioning as the linear operation unit for matrix multiplication. In this fiber-optics testbed, programmable MEMS VOAs mimic the PCM synaptic functions. III. Summation and detection: Due to constraints imposed by the polarization states of the polarized beam combiner, each neuron in our testbed implementation is limited to two input/synapse connections. Consequently, letter recognition tasks are executed using multiple partially connected layers to accommodate these experimental constraints (Fig. 3b-c). IV. Data collection and processing: Photodetector outputs are read by a digital multimeter and processed by a computer. The neurons are emulated via

computer using established experimental device data<sup>50</sup>. Details of the experimental setup are provided in the Methods and Supplementary Information Section 2, and the activation function in Supplementary Information Section 6.

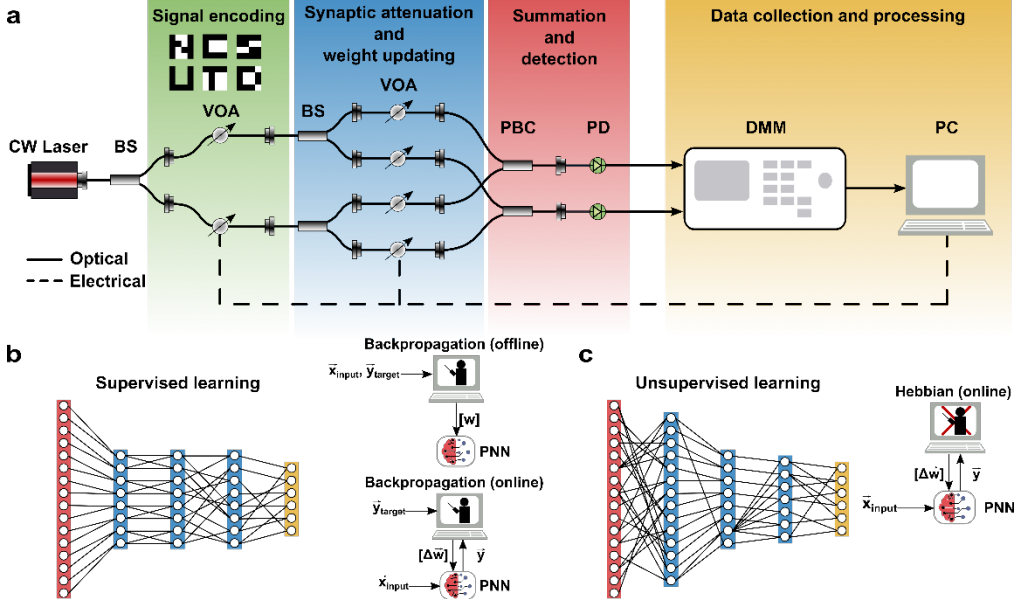


Fig. 3 Fiber-optics-based DPNN experimental setup and network architectures. (a) Schematic of experimental setup. Components include: beam splitter (BS), variable optical attenuator (VOA), polarized beam combiner (PBC), photodetector (PD), digital multimeter (DMM), and computer (PC). Input signals are generated by a CW laser and encoded using two VOAs. A  $2 \times 2$  VOA array controls synaptic weights for matrix multiplication. Output power is combined using PBCs and detected by two PDs. Voltage data is collected and post-processed on a PC. (b) PNN structure for supervised letter recognition. For offline backpropagation learning, the weights are pre-computed and programmed to the PNN (brain). For online backpropagation, the weights are continually updated based on backpropagation performed on a PC. (c) PNN structure for unsupervised letter recognition. A purely optical learning circuit continually updates the weights according to a Hebbian learning rule; no PC is required.

Our proof-of-concept task focuses on recognizing six letters, “NCSUTD”, derived from the names of our institutions (NCSU and UTD). This is a non-trivial task due to significant similarities among pixel images of the letters, as shown by Dice coefficient calculations (see details in Supplementary Information Section 3). For example, the letter ‘S’ exhibits moderate to high similarity with 5 out of 6 letters (Dice coefficients  $> 0.6$ ). The network is designed to capture letter-specific features, comprising an input layer (Layer I) with 16 neurons representing a  $4 \times 4$ -pixel image, multiple hidden layers (Layers A, B, C) designed to extract distinctive letter characteristics, and an output layer (Layer O) with 6 neurons, each corresponding to one of the six letters of “NCSUTD” (Fig. 3 ).

#### 4.1. Demonstration of supervised learning and inference

To evaluate the proposed DPNN, we first assessed its ability to perform inference following conventional supervised learning. Due to experimental constraints that limit each neuron to only 2 inputs, we designed a  $16 \times 8 \times 8 \times 8 \times 6$  neural network. This network structure accommodates our setup while ensuring that each of the six output neurons receives information from all 16 input neurons representing a  $4 \times 4$ -pixel image. During inference, the objective is to activate a single output neuron that outputs a high value, indicating a recognized input letter. For example, an output value of ‘1’ from the first neuron indicates recognition of the letter “N”, with similar mappings for other letters.

We first trained the DPNN offline with conventional backpropagation. To perform inference, the  $2 \times 2$  VOA synapse unit of Fig. 3a was reused and reprogrammed with attenuation values corresponding to the synaptic weights. Outputs from all intermediate hidden layers were measured by photodetectors and processed through a nonlinear activation function. The output values from the previous layer's neurons then served as input to the subsequent layers. The experimental results are summarized in Fig. 4a, with the output probabilities shown for each neuron, corresponding to the six input letters. Each row of the table represents the output neurons associated with the same input letter. As the diagonal cells exhibit the highest values, this experiment shows that the DPNN has correctly recognized the letters.

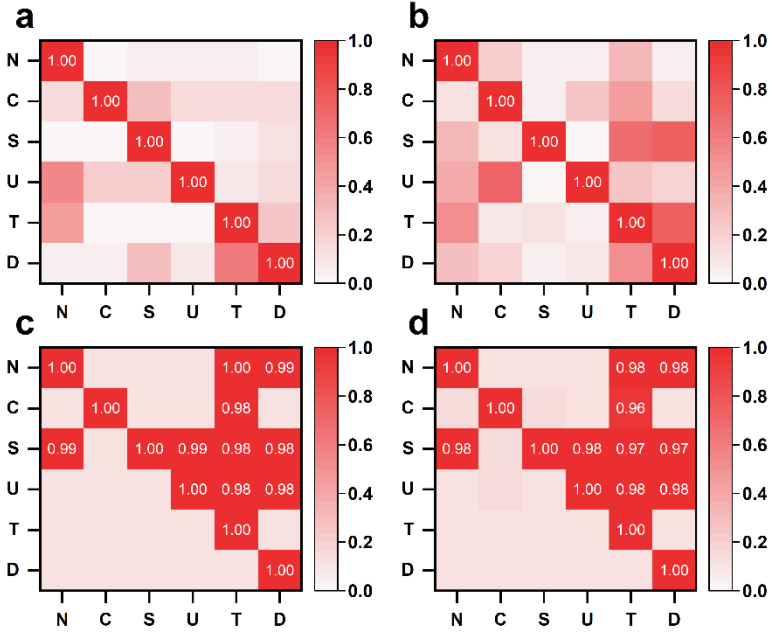


Fig. 4 The experimental recognition results, shown via the normalized output power distribution after training. The input letters are labeled on the y-axis, and the output letters are labeled on the x-axis. In all four panels, the diagonal elements attain the highest values, indicating 100% recognition accuracy. (a) Offline supervised learning; (b) Online supervised learning; (c) Offline unsupervised learning; (d) Online unsupervised learning.

Next, we implemented supervised online learning with a hardware-in-the-loop configuration, representing a significant step toward fully autonomous training. This approach leverages the outputs of the forward pass during inference to perform real-time training, eliminating the need for explicit readout of synapse weights. Using backpropagation, the synaptic weights (emulated by the VOAs) were continuously adjusted, namely, decremented (representing crystallization of PCM) or reset (representing amorphization of PCM) based on in-situ inference error gradient descent. The experimental results, depicted in Fig. 4b, revealed a steady decrease in the squared error sum of the output and a rapid increase in the recognition rate, reaching 100% within 100 epochs. Because training terminated upon achieving a 100% recognition rate, further optimization of synaptic weights to refine the output probability distribution was not performed. Consequently, the output power distribution in the online learning results (Fig. 4b) is less pronounced than in its offline counterpart (Fig. 4a). Nevertheless, this result demonstrates the effectiveness and potential of online learning in our experimental setup.

#### 4.2. Demonstration of unsupervised learning

To enable unsupervised learning in our DPNN, we used the neural network structure of Fig. 3, and importantly, replaced the global backpropagation used in supervised learning with the local feedback learning illustrated in Fig. 1a. Our approach applies a Hebbian learning rule<sup>46,47</sup> based solely on internal network dynamics (detailed in the Methods section and Supplementary Information Section 1) that clusters inputs without requiring labeled data or supervision. This capability is a core feature of unsupervised learning, as it allows the network to autonomously discover patterns and relationships within the input data without prior knowledge of class labels. Since unsupervised learning does not include labeling, we assume a simple output layer trained to label the unsupervised network's outputs.

The results of the offline unsupervised letter recognition task are summarized in Fig. 4c. As expected, compared to the supervised learning results, the output power distributions exhibit less pronounced separation; this is particularly noticeable for the letter "S," which shares significant pixel overlap with other letters in our dataset. This reduced divergence is a direct consequence of the specific constraints of our experimental setup. Specifically, the dynamic range of the synaptic weights was considerably smaller in the unsupervised experiments. While the supervised learning experiments used the full 40 dB attenuation range of the VOA, the VOAs in the unsupervised learning configuration emulated a PCM waveguide synapse, providing only a ~37% transmission contrast between its fully amorphous and crystalline states in our setup for a 5  $\mu\text{m}$ -long PCM cell. This limited dynamic range stemmed from finite absorption in the crystalline state and the potentially incomplete phase transition across the PCM cell due to the optical pulses' finite energy. This reduced dynamic range inherently increases the system's susceptibility to noise and polarization crosstalk, thereby impacting inference accuracy.

Finally, we demonstrated online unsupervised Hebbian learning in our DPNN. In this configuration, the computer served solely as temporary data storage and emulated the ReLU-like nonlinear activation function of a PCM microring neuron. The synaptic weights, implemented via the VOAs, were updated in real-time according to the PCM synapse weight updating rules detailed in Section 2 and Supplementary Information Section 1. All six letter patterns were repeatedly presented to the physical PNN. As shown in **Error! Reference source not found.**, the system successfully classified all six letters, highlighting the robustness of our online unsupervised learning approach. Notably, online learning inherently incorporates additional sources of randomness absent in offline training, including laser output power error (0.02 dB), VOA repeatability limitations (0.1 dB), fiber optic insertion losses, and polarization crosstalk (See Supplementary Information Section 4). While these factors initially contributed to the misclassification of the letter "N" in the offline unsupervised learning (Fig. 4c), the online learning process successfully adapted and corrected this misclassification, demonstrating its robustness in overcoming physical photonic hardware limitations.

## 5. Discussion

This work presents a novel DPNN architecture and validates its feasibility through the experimental demonstration of a fiber-optics-based PNN. The multilayer photonic crossbar architecture supports real-time unsupervised learning by incorporating non-volatile PCM synapses and local optical feedback. During learning, the feedback loop temporally overlaps input and feedback signals, enabling continuous synaptic weight updates based on both the optical energy and the current PCM state. We successfully demonstrated Hebbian learning for a letter-recognition task entirely in the optical domain, highlighting its potential for scalable, energy-efficient photonic computing.

The core innovation of this work lies in designing Hebbian learning directly in the photonic domain, by leveraging local optical feedback and the thermal-optical properties of PCMs. This approach enables unsupervised online learning without relying on O-E-O conversions or labeled datasets, marking a key step toward autonomous, adaptive DPNNs. Inference is

achieved through passive optical transmission that minimizes energy consumption at the speed of light. These features collectively enable the development of low-power PNNs that learn autonomously.

Unlike previous PNNs that rely on external supervision, electrical feedback, or offline training, our approach provides a fully integrated photonic learning mechanism operating entirely in the optical domain. The choice of PCM-based synapses provides non-volatility and eliminates the need for continuous energy input to maintain synaptic weights, thus offering both energy efficiency and stability. While the experimental demonstration shown here utilizes a fiber-optics system and only emulates the PCM functions, the underlying principles are transferable to scalable on-chip implementations. Once realized on-chip on a silicon photonics platform, further efforts will aim to scale the system to larger networks as well as to integrate faster optical switching components.

## 6. Methods

### *Measurement setup*

The experimental setup (Supplementary Fig. S3) for the DPNN is built using commercially available fiber-optics components. Optical synapses are implemented using a 6-channel micro-electromechanical systems (MEMS) VOA module by Dicon Fiberoptics. Two channels are dedicated to modulating the input signal amplitude, while the remaining four are configured in a  $2 \times 2$  arrangement to adjust synaptic weights by controlling input signal attenuation. The MEMS VOAs, with their modest response time ( $< 2$  ms) and high durability ( $> 1 \times 10^9$  cycles), enable real-time online learning for letter recognition tasks. Functioning as non-volatile, reconfigurable PCM optical synapses, these VOAs can be tuned via an RS-232 control interface, supporting both offline and online learning.

Optical neurons, which implement nonlinear activation functions, are simulated using software-based neuron models with inverse-sigmoid and ReLU-like activation functions. Due to phase differences between signals traveling through different optical paths, conventional beam combiners posed challenges in power combining. To mitigate such interference, polarized beam combiners are used to merge signals before photodetector detection. A comprehensive analysis of output power stability and polarization crosstalk is provided in the Supplementary Information Section 4.

Given the constraints of available experimental resources, a  $2 \times 2$  synapse unit has been reused repeatedly to construct the PNN, with intermediate values from hidden layers temporarily stored in computer memory.

### *Training algorithm – the backpropagation method*

For supervised learning, we employ classical backpropagation based on gradient descent. The cost function, or error, measures the difference between the expected ( $Y$ ) and actual ( $O_a$ ) neuron output values:

$$E = Y - O_a$$

Whereas the gradient is calculated as a function of the errors:

$$dO = df(O) \times E$$

This gradient is then backpropagated through the network using the chain rule:

$$dC = df(C) \times (dO \times W4)$$

$$dB = df(B) \times (dC \times W3)$$

$$dA = df(A) \times (dB \times W2)$$

The weights for each layer of synapses are updated using the following rule:

$$W4 = \alpha \times W4 + \eta \times C_a \times dO$$

$$W3 = \alpha \times W3 + \eta \times B_a \times dC$$

$$W2 = \alpha \times W2 + \eta \times A_a \times dB$$

$$W1 = \alpha \times W1 + \eta \times X \times dA$$

Where momentum  $\alpha = 1$  and learning rate  $\eta = 0.065$  are both constants. A, B, C, and O represent the output vector for different hidden and output layers, while  $A_a$ ,  $B_a$ , and  $C_a$  represent the output vectors after the nonlinear activation has been applied.

#### *Learning algorithm –local Hebbian rule*

For unsupervised learning, we employ a Hebbian rule. Synapse updates are based on the input signal, local feedback signal, and the current synaptic weight. Given the fixed timing relationship between input and output signals, synaptic weight updates depend solely on the combined amplitude of the input and feedback signals. Three distinct outcomes are possible: no action (weight maintenance), crystallization (weight decrease), and amorphization (weight increase). Unlike conventional backpropagation, which relies on global feedback, our Hebbian rule relies on local feedback. Additionally, it avoids differential computations, thus eliminating the need for on-chip electronic components, making it ideally suited for all-optical neural network implementations. The weight update  $\Delta w$  is a function of the i-th input presynaptic signal in the N-th layer  $x_{i,N}$ , the feedback signal in the N-th layer  $y_N$ , and the current synaptic weight  $w$ ,  $\Delta w = f(x_{i,N}, y_N, w)$ .

#### **Acknowledgments**

This research was supported by two National Science Foundation (NSF) CAREER Awards (ECCS- 2209871 and CCF- 2146439), the Army Research Office (ARO) Young Investigator Program (W911NF-19-1-0303), and Defense Advanced Research Projects Agency (DARPA) MTO HR0011-25-3-0188.

#### **Author contributions**

X.L., J.S.F., and Q.G. conceived the PNN design. X.L. designed the experimental setup and performed all measurements with assistance from A.C. D.B. developed the training algorithm, with contributions from P.Z. and W.H.B. J.S.F. and Q.G. supervised the project. All authors participated in data analysis. X.L. wrote the manuscript with contributions from all authors.

#### **Competing financial interests**

The authors declare no competing interests.

#### **Additional information**

#### **References**

1. Nandakumar, S. R., Kulkarni, S. R., Babu, A. V. & Rajendran, B. Building brain-inspired computing systems: Examining the role of nanoscale devices. *IEEE Nanotechnol. Mag.* **12**, (2018).
2. Shastri, B. J. *et al.* Photonics for artificial intelligence and neuromorphic computing. *Nature Photonics* vol. 15 Preprint at <https://doi.org/10.1038/s41566-020-00754-y> (2021).

3. Schuman, C. D. *et al.* Opportunities for neuromorphic computing algorithms and applications. *Nature Computational Science* vol. 2 Preprint at <https://doi.org/10.1038/s43588-021-00184-y> (2022).
4. Kudithipudi, D. *et al.* Neuromorphic computing at scale. *Nature* **637**, 801–812 (2025).
5. Painkras, E. *et al.* SpiNNaker: A 1-W 18-Core System-on-Chip for Massively-Parallel Neural Network Simulation. *IEEE J. Solid-State Circuits* **48**, 1943–1953 (2013).
6. Akopyan, F. *et al.* TrueNorth: Design and Tool Flow of a 65 mW 1 Million Neuron Programmable Neurosynaptic Chip. *IEEE Transactions on Computer-Aided Design of Integrated Circuits and Systems* **34**, 1537–1557 (2015).
7. Davies, M. *et al.* Loihi: A Neuromorphic Manycore Processor with On-Chip Learning. *IEEE Micro* **38**, 82–99 (2018).
8. Neckar, A. *et al.* Braindrop: A Mixed-Signal Neuromorphic Architecture With a Dynamical Systems-Based Programming Model. *Proceedings of the IEEE* **107**, 144–164 (2019).
9. Pei, J. *et al.* Towards artificial general intelligence with hybrid Tianjic chip architecture. *Nature* **572**, 106–111 (2019).
10. Wan, W. *et al.* A compute-in-memory chip based on resistive random-access memory. *Nature* **608**, 504–512 (2022).
11. Müller, E. *et al.* The operating system of the neuromorphic BrainScaleS-1 system. *Neurocomputing* **501**, 790–810 (2022).
12. Richter, O. *et al.* DYNAP-SE2: a scalable multi-core dynamic neuromorphic asynchronous spiking neural network processor. *Neuromorphic Computing and Engineering* **4**, 014003 (2024).
13. Nahmias, M. A. *et al.* Photonic Multiply-Accumulate Operations for Neural Networks. *IEEE Journal of Selected Topics in Quantum Electronics* **26**, (2020).
14. Tait, A. N., Nahmias, M. A., Shastri, B. J. & Prucnal, P. R. Broadcast and weight: An integrated network for scalable photonic spike processing. *Journal of Lightwave Technology* **32**, (2014).
15. Shen, Y. *et al.* Deep learning with coherent nanophotonic circuits. *Nat. Photonics* <https://doi.org/10.1038/nphoton.2017.93> (2017) doi:10.1038/nphoton.2017.93.
16. Lin, X. *et al.* All-optical machine learning using diffractive deep neural networks. *Science (1979)* **361**, (2018).

17. Feldmann, J., Youngblood, N., Wright, C. D., Bhaskaran, H. & Pernice, W. H. P. All-optical spiking neurosynaptic networks with self-learning capabilities. *Nature* <https://doi.org/10.1038/s41586-019-1157-8> (2019) doi:10.1038/s41586-019-1157-8.
18. Feldmann, J. *et al.* Parallel convolutional processing using an integrated photonic tensor core. *Nature* **589**, (2021).
19. Ashtiani, F., Geers, A. J. & Aflatouni, F. An on-chip photonic deep neural network for image classification. *Nature* **606**, 501–506 (2022).
20. Wu, T., Menarini, M., Gao, Z. & Feng, L. Lithography-free reconfigurable integrated photonic processor. *Nature Photonics* **2023** 1–7 (2023) doi:10.1038/s41566-023-01205-0.
21. Bandyopadhyay, S. *et al.* Single-chip photonic deep neural network with forward-only training. *Nat. Photonics* **18**, 1335–1343 (2024).
22. Shi, W., Huang, Z., Fu, T. & Chen, H. Review of nonlinear activation functions in optical neural networks. *Advanced Photonics* **7**, 064004 (2025).
23. Tait, A. N. *et al.* Neuromorphic photonic networks using silicon photonic weight banks. *Sci. Rep.* **7**, (2017).
24. Hamerly, R., Bernstein, L., Sludds, A., Soljačić, M. & Englund, D. Large-Scale Optical Neural Networks Based on Photoelectric Multiplication. *Phys. Rev. X* **9**, (2019).
25. De Marinis, L., Cococcioni, M., Castoldi, P. & Andriolli, N. Photonic Neural Networks: A Survey. *IEEE Access* <https://doi.org/10.1109/ACCESS.2019.2957245> (2019) doi:10.1109/ACCESS.2019.2957245.
26. Bernstein, L. *et al.* Single-shot optical neural network. *Sci. Adv.* **9**, (2023).
27. Wright, L. G. *et al.* Deep physical neural networks trained with backpropagation. *Nature* **601**, (2022).
28. Zhou, W. *et al.* In-memory photonic dot-product engine with electrically programmable weight banks. *Nature Communications* **2023** *14*:1 **14**, 1–10 (2023).
29. Nøkland, A. Direct feedback alignment provides learning in deep neural networks. in *Advances in Neural Information Processing Systems* (2016).
30. Lillicrap, T. P., Cownden, D., Tweed, D. B. & Akerman, C. J. Random synaptic feedback weights support error backpropagation for deep learning. *Nat. Commun.* **7**, (2016).
31. Filipovich, M. J. *et al.* Silicon Photonic Architecture for Training Deep Neural Networks with Direct Feedback Alignment. <https://doi.org/10.48550/arxiv.2111.06862> (2021) doi:10.48550/arxiv.2111.06862.

32. Cheng, Z., Ríos, C., Pernice, W. H. P., David Wright, C. & Bhaskaran, H. On-chip photonic synapse. *Sci. Adv.* <https://doi.org/10.1126/sciadv.1700160> (2017) doi:10.1126/sciadv.1700160.
33. Duan, B., Wu, B., Chen, J. H., Chen, H. & Yang, D. Q. Deep Learning for Photonic Design and Analysis: Principles and Applications. *Frontiers in Materials* vol. 8 Preprint at <https://doi.org/10.3389/fmats.2021.791296> (2022).
34. Wuttig, M. & Yamada, N. Phase-change materials for rewriteable data storage. *Nat. Mater.* **6**, (2007).
35. Wong, H. S. P. *et al.* Phase change memory. *Proceedings of the IEEE* **98**, 2201–2227 (2010).
36. Burr, G. W. *et al.* Phase change memory technology. *Journal of Vacuum Science & Technology B, Nanotechnology and Microelectronics: Materials, Processing, Measurement, and Phenomena* **28**, (2010).
37. Ríos, C. *et al.* Integrated all-photonic non-volatile multi-level memory. *Nat. Photonics* <https://doi.org/10.1038/nphoton.2015.182> (2015) doi:10.1038/nphoton.2015.182.
38. Wuttig, M., Bhaskaran, H. & Taubner, T. Phase-change materials for non-volatile photonic applications. *Nature Photonics* vol. 11 Preprint at <https://doi.org/10.1038/nphoton.2017.126> (2017).
39. Ríos, C. *et al.* In-memory computing on a photonic platform. *Sci. Adv.* **5**, (2019).
40. Zheng, J. *et al.* Nonvolatile Electrically Reconfigurable Integrated Photonic Switch Enabled by a Silicon PIN Diode Heater. *Advanced Materials* <https://doi.org/10.1002/adma.202001218> (2020) doi:10.1002/adma.202001218.
41. Lee, J. S., Farmakidis, N., Wright, C. D. & Bhaskaran, H. Polarization-selective reconfigurability in hybridized-active-dielectric nanowires. *Sci. Adv.* **8**, 9459 (2022).
42. Miscuglio, M. *et al.* Massively parallel amplitude-only Fourier neural network. *Optica* **7**, (2020).
43. Ashtiani, F., Geers, A. J. & Aflatouni, F. An on-chip photonic deep neural network for image classification. *Nature* **606**, 501–506 (2022).
44. Zhou, W. *et al.* In-memory photonic dot-product engine with electrically programmable weight banks. *Nature Communications* **2023 14:1 14**, 1–10 (2023).
45. Ma, Y. *et al.* Ultralow loss single layer submicron silicon waveguide crossing for SOI optical interconnect. *Opt. Express* **21**, (2013).
46. Querlioz, D. *et al.* Bioinspired networks with nanoscale memristive devices that combine the unsupervised and supervised learning approaches. in *2012 IEEE/ACM*

*International Symposium on Nanoscale Architectures (NANOARCH)* 203–210 (2012). doi:10.1145/2765491.2765528.

47. Zhou, P. *et al.* Neuromorphic Hebbian learning with magnetic tunnel junction synapses. *Communications Engineering* **4**, 142 (2025).
48. Sebastian, A., Le Gallo, M. & Krebs, D. Crystal growth within a phase change memory cell. *Nat. Commun.* **5**, 4314 (2014).
49. Wang, Y., Ning, J., Lu, L., Bosman, M. & Simpson, R. E. A scheme for simulating multi-level phase change photonics materials. *NPJ Comput. Mater.* **7**, 183 (2021).
50. Shi, B., Calabretta, N. & Stabile, R. First demonstration of a two-layer all-optical neural network by using photonic integrated chips and SOAS. in *IET Conference Publications* vol. 2019 (2019).